Seyedmajid Mehrnia*
Peter F. Pelz*

Tribological Design by Molecular Dynamics Simulation: Influence of the Molecular Structure on Wall Slip and Bulk Shear

The tribological properties of a complex branched-hydrocarbon oil under shear in a gap between smooth iron atom surfaces were studied by large-scale molecular dynamics (MD) simulation. The liquid was a nonpolar lubricant, i.e. a polyalphaolefin (PAO) oil mixture of 1-decane dimer, trimer, and tetramer molecules. The rheological characteristics of the lubricant, including the shear stress and viscosity as well as the relaxation time of the liquid molecule, were calculated. The results show that, as the number of branches of the liquid molecule increases, the shear stresses and the wall slip increase. However, for a mixture fluid containing three different branched molecules, the wall slip decreases in comparison to a liquid consisting of only one kind of branched molecule.

Keywords: Liquid films, Polyalphaolefins, Shear flows, Slip velocity, Viscosity

Received: September 18, 2022; *accepted:* September 23, 2022

DOI: 10.1002/ceat.202200448

1 Introduction

Different liquid lubricants are utilized on sliding surfaces and rotating parts in order to reduce the unfavorable consequences of friction. Despite this, most researchers are trying to decrease the usage of lubricant fluids because of their undesirable influence on the environment. The two factors contributing to friction in tribology systems are the bulk shear and the wall slip, which were studied in this research.

The concept of apparent and real measurements has been confirmed to be practical in rheology and is thus employed here also in the context of molecular dynamics (MD) tribology. Assuming a fluid film between two parallel walls having the distance h and sliding relatively to each other with velocity U, the apparent shear rate is $\dot{\gamma}_{app} = U/h$ and the apparent shear stress is $\tau_{app} = \mu\,\dot{\gamma}_{app}$. For any (in the time average) stationary Couette flow, the real shear stress $\tau(z) = \tau_w$ is constant across the channel height $0 \le z \le h$ and equal to the wall shear stress τ_w. For a small Reynolds number, the shear stress is, in the complete flow field, dominated by molecular (i.e. viscous) forces and the result of the constant shear stress is a constant field of shear rate $\tau = \tau_w = \mu\dot{\gamma} = \text{const.}$ [1].[1)]

For low-Reynolds number flow, Fig. 1 schematically presents two facts: Firstly, the wall slip increases the effective gap height from h to $h_{app} = h + 2\lambda$; secondly, the real shear is smaller than the effective shear rate $\dot{\gamma} = \dot{\gamma}_w = U/h_{app} < U/h$ and the real shear stress is smaller than the effective shear stress $\tau < \tau_{app}$ (see Fig. 1). Navier formulated the linear slip boundary condition $\tau_w = k u_s$ as a constitutive equation relating the wall shear stress

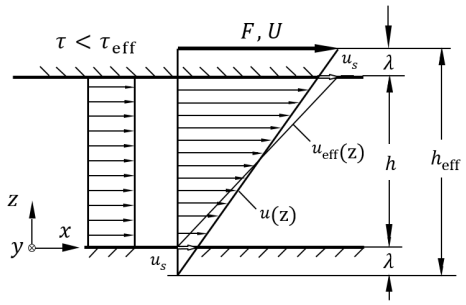

Figure 1. Increase of the effective gap height due to molecular slip at the wall.

τ_w to the tangential slip velocity $u_s = u - u_w$. The latter is the discrepancy between the absolute velocity u of a fluid molecule tangential to the wall and the lateral velocity u_w of the wall. Combining Navier's law for wall slip with Newton's law for shear $\tau_w = \mu\dot{\gamma}_w$ at the shear rate $\dot{\gamma}_w = \mathrm{d}u/\mathrm{d}z$ at the wall $z = 0$ yields $u_s = \lambda\dot{\gamma}_w$. Here, the slip length $\lambda = \mu/k$ is the ratio of the dynamic viscosity μ and the friction factor k.

It is advantageous to shed some light on Newton's constitutive equation $\tau = \mu\dot{\gamma}$ for shear and Navier's boundary condition $\tau_w = k u_s$ for a wall slip from the outlook of phenomenological tribology and rheology. The viscosity μ and the friction factor

1) List of symbols at the end of the paper.

Seyedmajid Mehrnia, Dr. Peter F. Pelz
Seyedmajid.mehrnia@fst.tu-darmstadt.de,
Peter.pelz@fst.tu-darmstadt.de
Chair of Fluid Systems, Technische Universität Darmstadt, Otto-Berndt-Straße 2, 64287 Darmstadt, Germany.

k, or the equivalent slip length $\lambda = \mu/k$, are functions of the shear rate $\dot{\gamma}$; the temperature T and the molecular properties are given by the (weight-averaged) molecular weight M and the number of molecule branches.

$$\text{shear } \mu = \mu(\dot{\gamma}, T, M), \ \text{slip } \lambda = \lambda(\dot{\gamma}, T, M, \text{solid}) \quad (1)$$

The liquid used in this research work is a polyalphaolefin (PAO), the base of synthetic lubricants employed in technical applications, which is a mixture of olefin dimers, trimers, and tetramers. The structures of the three molecules are shown in Fig. 2.

The wall sliding of lubricants including hydrocarbon oils in interaction with metal surfaces has already been studied in numerous research works. For example, a slip model was proposed for linear hydrocarbon lubricants confined between metal atom surfaces regarding the given surface parameters and the shear viscosity. However, this model is valid for ambient temperature, and the impact of the temperature on the slip relation was not included [2]. In another work, a linear hydrocarbon with the United-Atoms (UA) model was used for simulating iron with body-centered cubic lattice sliding walls. Two different temperatures were utilized for the fluid, but their effects on the wall slip were not noticed [3]. Ewen et al. [4] have studied the impact of the surfactant type and coverage on the slip behavior for *n*-hexadecane liquid, and the results showed that a higher slip length gives a lower friction. MD simulation of a hexadecane oil film while it is sheared between two metal surfaces was investigated to discover the effects of the shear rate, the film thickness, and the surface energy on the wall slip [5].

In this paper, a large-scale MD simulation of Couette flow was carried out to study the bulk shear and wall slip of a nonpolar lubricant, i.e. hydrocarbon oils, emphasizing the effect of the molecule branches interacting with smooth iron surfaces. This paper aims (1) to study the bulk shear including the viscosity and the relaxation time of three different branched molecules and (2) to investigate the wall slip of the branched hydrocarbon molecules at different temperatures. To achieve these aims, first, the method of the simulation is explained. Then, the results of the simulation for different branched molecules and temperatures are presented.

2 Simulation Method

MD was used as a tool for the simulation of the PAO-iron lubrication system in this research. The classical equation of motion for a system of atoms was solved to obtain the time evolution of the system. Definition of the potential energy functions is required to compute the forces of the system. In our MD simulation, the most accurate numerical scheme to simulate atomic motions is the Verlet algorithm employed in this simulation. Also, to decrease the calculation time, a "neighbor list" numerical scheme was applied. Statistical mechanics provided the concepts for describing macroscopic considerations in the classification of microscopic states by employing a constant-energy, constant-volume ensemble (NVE ensemble). The UA model was applied for atom groups (CH_3, CH_2, and CH) to decrease the computational time. Besides, a Langevin thermostat supported the lubricant atoms in recovering the desired temperature more precisely. The structures of the three branched molecules are shown in Fig. 2. In this paper, it was assumed that the base PAO is a mixture of 1-decane trimer (60 %), tetramer (30 %), and dimer (10 %).

In Fig. 3, the 1-decane tetrameric molecules were confined between body-centered cubic iron atoms with a lattice constant of 0.286 nm. The thickness of each metal layer is 2 nm. The total number of the liquid molecule is 24 157 and the thickness of the oil film is 20 nm. Apart from the situation depicted in Fig. 3, the gap width is varied. The temperature changed in the range from 20 to 60 °C. The appropriate shear rate values to capture the initial Newtonian plateau of PAO lubricant oils at room temperature are the values below $5\times10^8\,s^{-1}$ at ambient temperature [1]. For this study, this is important since the apparent shear rate is lower than this critical shear rate.

All models were designed by Avogadro software [6] and then assembled and optimized by the Packmol software [7]. The model utilized for the liquid molecules is a full atom style model that includes bond stretching, bending, and torsion. The MD equations of motion were integrated using the velocity-Verlet algorithm with an integration timestep of 1.0 fs for the selected force field. The MD modeling in this research was performed by the LAMMPS MD simulator, an open-source code [8]. Updating the velocity and positions of atoms in the group for each timestep was performed by a constant NVE integration. The initial macroscopic variables of the microcanonical ensemble are the number of atoms in the system (N), the volume of the system (V), and the energy in the system (E),

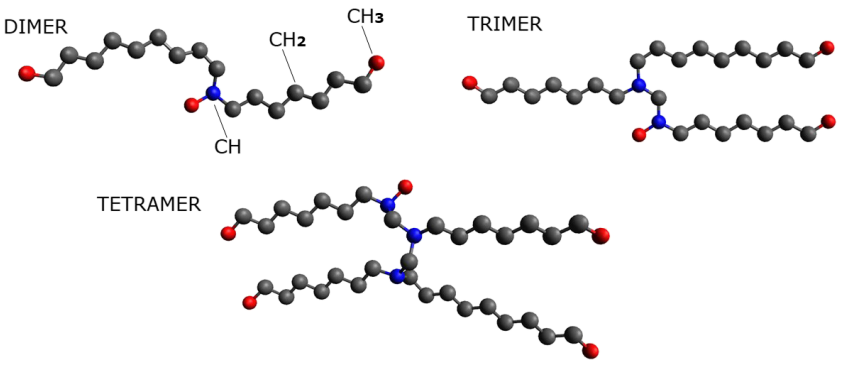

Figure 2. Structures of the 1-decane dimer, trimer, and tetramer molecules.

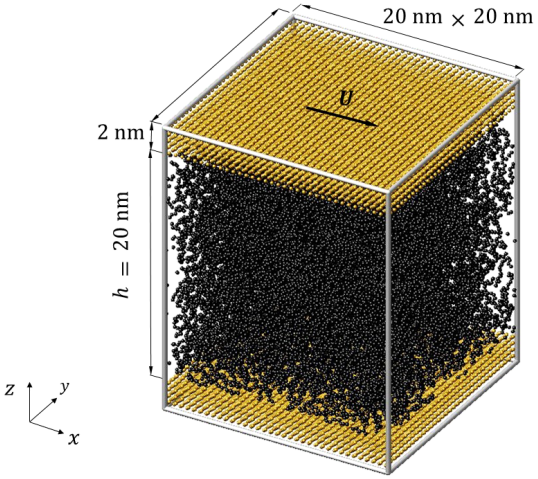

Figure 3. Simulation box of the 1-decane tetrameric molecules confined between body-centered cubic Fe atoms with a lattice constant of 0.286 nm. The upper surface is moving and the lower surface is stationary.

which are assumed to be fixed. NVE creates a system trajectory compatible with the microcanonical ensemble [9]. At the beginning of the simulation, the system was relaxed to equilibrium at 0.05 ns. Hence, the system achieved a thermodynamic steady state. Through all modelings, the temperature is uniformly controlled by a Langevin thermostat. This thermostat simulates a conductive heat flux through the walls and guarantees heat removal from the fluid.

Past studies have shown that UA Coarse-Grain models can accurately depict the behavior of hydrocarbons at various pressures. For an MD simulation, the selection of the appropriate force field is important. One of the known force fields for a branched-hydrocarbon oil is the NERD force field, which can be extended to suit alpha-olefins [10, 11]. For the coarse-graining, CH_3, CH_2, and CH groups are modeled as single interaction sites. The NERD force field employs a Lennard-Jones (LJ) potential for non-bonded interaction sites, excluding intramolecular interactions within three bonds of the same molecule. A standard LJ 12-6 potential as below is used for this non-bonded interaction (Eq. (2)).

$$E_{LJ}(r) = 4\varepsilon\left[\left(\frac{\sigma}{d}\right)^6 - \left(\frac{\sigma}{d}\right)^{12}\right],\ d < d_c \tag{2}$$

where d is the distance among two pseudo-atoms, ε is an energy parameter, and σ is specified as the length at which the intermolecular energy within the two pseudo-atoms is zero. Thus, it could be called the van der Waals radius. ε is the well depth and a measure of attraction between two pseudo-atoms. In addition, d_c known as cutoff radius for the LJ interaction potential is set to 1.15 nm, where the interaction parameters for unlike pairs are calculated through the Lorentz-Berthelot combination rules (Eqs. (3) and (4)) [10]. Non-bonded LJ potential parameters are tabulated in Tab. 1.

$$\sigma_{ij} = \frac{\sigma_{ii} + \sigma_{jj}}{2} \tag{3}$$

Table 1. Non-bonded LJ potential parameters [10].

UA group	ε [meV]	σ [Å]
CH	3.42	3.85
CH_2	3.95	3.93
CH_3	8.96	3.91
Fe	40.98	2.32

$$\varepsilon_{ij} = \sqrt{\varepsilon_{ii}\varepsilon_{jj}} \tag{4}$$

For bond stretching and angle bending interactions, harmonic potentials are employed:

$$u_r = \frac{k_r}{2}(r - r_0)^2 \tag{5}$$

$$u_\theta = \frac{k_\theta}{2}(\theta - \theta_0)^2 \tag{6}$$

with r_0 and θ_0 being the equilibrium bond length and angle, respectively. The torsional potential is described using Eq. (7).

$$u_\phi = V_0 + V_1(1 + \cos\phi) + V_2(1 - \cos 2\phi) + V_3(1 + \cos 3\phi) \tag{7}$$

All the parameters for the intramolecular potential energy functions can be found in Tab. 2.

Table 2. Intramolecular potential energy function parameters [10].

Bond stretching potential	
$k_r = 8.31568$ eV Å^{-2}	$r_0 = 1.54$ Å
Bond bending potential	
$k_\theta = 5.39$ eV rad^{-2}	$\theta_0 = 1.99$ rad
Torsional potential	
CH_x-CH_2-CH_2-CH_y	
$V_0 = 0$ meV	$V_1 = 31$ meV
$V_2 = -23$ meV	$V_3 = 68$ meV
CH_x-CH_2-CH-CH_y	
$V_0 = 122$ meV	$V_1 = 34$ meV
$V_2 = 12$ meV	$V_3 = -250$ meV

For modeling the walls, simple spring potentials can be employed or a more sophisticated force field for metals can be chosen. For this simulation, the embedded-atom method (EAM) potential was used to model the iron walls. The EAM is a popular choice for modeling the force field of metals and alloys. It was developed by Daw and Baskes [12] and is based on the density-functional theory for calculating the properties

of realistic metal systems. Embedding energy coupled with a pair potential was used to model the bulk material.

3 Results

The precision of the MD results is highly related to the force field of atoms interaction, a good convergence achievement, and to how well the microcanonical ensembles are applied. Furthermore, timestep selection for MD simulation is critical in starting the simulation. The force field specifies the required timestep. In general, if atoms or molecules move too much within two integrations, the simulation is unconvinced. In many studies related to a hydrocarbon lubricant sheared by non-equilibrium MD (NEMD), the simulation timestep was 1.0 fs [2].

The density distribution in Fig. 4 shows the explicit molecular layering of the three different branched PAO molecules. Areas near the surfaces are the adsorption layer with elevated mutation and oscillations in the mass density profiles. It can be noticed that the 1-decane dimer has the lowest value of density due to the smaller molecular mass. It is also perceived that the atomic boundary layers had slightly higher density peaks for the tetramer than the atomic boundary layers of the trimer. The peak splitting near the surfaces in the mass density profile is notable. This can be illustrated by the lower area of repulsion of the UA atoms where these pseudo-atoms could closely approach the walls, possibly binding more firmly to the metal atoms. The measured mass density of the PAO 6 is 0.835 g mL^{-1} at ambient temperature. The averaged densities of the three molecule structures from the MD simulation in Fig. 4 are in agreement with the measured density.

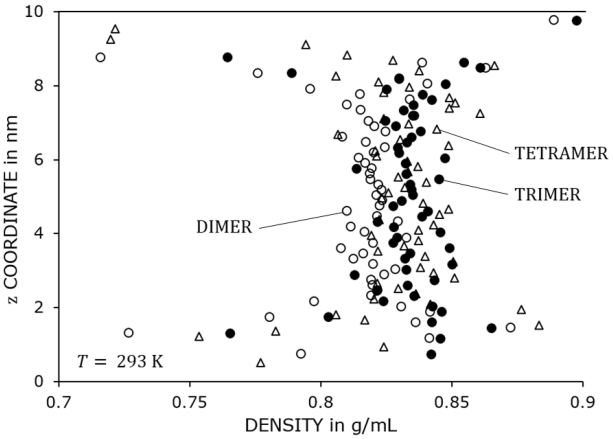

Figure 4. Mass density distribution of the three different structures of 1-decane.

3.1 Bulk Shear

The shear viscosity of the fluid μ was calculated as the ratio of the shear stress $\tau = \sigma_{xz}$ and the apparent shear rate $\mu = \tau/\dot{\gamma}$ [5]. The general equation of the stress tensor of many-body interaction potentials under periodic boundary conditions was used to calculate the shear stress [13]. Fig. 5 shows the calculated

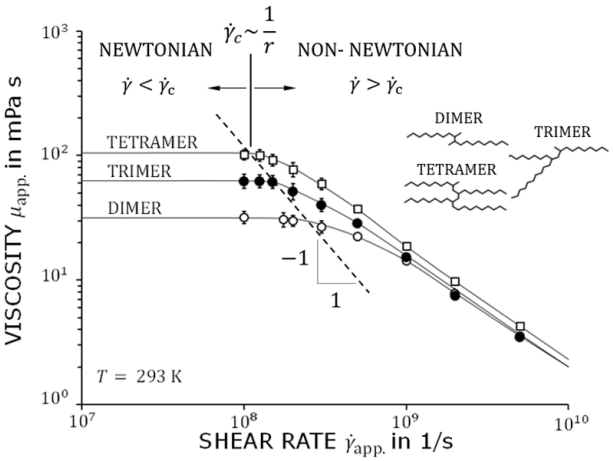

Figure 5. Dynamic viscosity at different apparent shear rates for the three kinds of branched molecules.

dynamic viscosity versus the various shear rates at a temperature of $T = 293$ K. The error bars shown in Fig. 5 were calculated over a time interval of 5 ns. The measured Newtonian viscosity μ_0 of PAO 6 in a rheometer was about 40 mPa s at the temperature of 293 K. As the PAO 6 oil was a mixture of 1-decane tetramers, trimers, and dimers, an imprecise comparison can be made. The calculated Newtonian viscosities for the 1-decane dimers, trimers, and tetramers are 31, 62, and 102 mPa s, respectively. The calculated critical shear rates were in the order of 10^8 s^{-1}. Here it should be mentioned that the critical shear rate increases further with increasing temperature. As can be seen in Fig. 5, the viscosity increased as the number of branches increased. It can also be seen that the critical shear rate is lower for molecules that have more branches. This means that, as the number of branches increases, the shear-thinning begins at a lower shear rate.

Most modern alkene-based lubricant fluids, such as PAO oils, exhibit both Newtonian and non-Newtonian behavior. At low shear rates, the viscosity is constant (Newtonian plateau). After a critical shear rate $\dot{\gamma}_c$ is surpassed, the viscosity decreases rapidly (shear-thinning). Importantly, rheological properties are influenced by the molecular structure of the lubricant [14]. Models that incorporate the molecular weight are the Mark-Houwink relation and the Rouse model. Both can be used to relate the critical shear rate to the relaxation time of a polymeric fluid [15]. The Rouse model originally described the melt of short, unentangled polymer chains. However, since hydraulic fluids also often consist of relatively short, unentangled polymer chains, the Rouse model is applicable as well. Thus, the Rouse model can also be used to find the critical shear rate in hydrocarbon oils, which constitutes an inversely proportional relationship between the shear rate and the relaxation time r of the molecules in an equilibrium condition [15] (Eq. (8)).

$$\dot{\gamma}_c \propto \frac{1}{r} \tag{8}$$

For short-length molecules such as PAO oils, the relaxation time r and the dynamic viscosity μ are proportional to the molecular weight, being a measure for the molecular size:

$\mu \infty M$, $r \infty M$. The molecular masses of the 1-decane dimer, trimer, and tetramer are 283, 423, and 563 g mol^{-1}, respectively. For $\dot{\gamma} r << 1$ there is no shear rate dependence of shear and slip. The relaxation time is the time for the return of a perturbed system to equilibrium. In this MD simulation, the relaxation time of the molecule for the first Newtonian plateau is given by the inverse critical shear rate $\dot{\gamma}_c$, i.e., in 10 ns. With increasing number of molecule branches as well as molecular mass, the relaxation time of the molecule is elevated. Also, it should be noted that, with increasing temperature, the critical shear rate is higher, and thus the relaxation time should be shorter. In a practical lubrication context, the gap height is larger than $h > 1\,\mu m$ and the velocity is smaller than 1 m s^{-1}. Thus, the apparent shear rate is smaller than 10^6 s^{-1}. Hence, a shear rate dependence is mostly not given.

Furthermore, the Einstein-Debye equation can be used to calculate the relaxation time, combined with Eq. (8) in relation to the molecular weight of the molecules and temperatures as shown in Eq. (9) [14].

$$r = \frac{\mu M}{\rho R T} \tag{9}$$

where ρ is the density, T is the temperature, R is the universal gas constant, μ is the Newtonian viscosity, and M is the molecular weight. Using Eq. (9), the relaxation time for PAO 6 can be estimated at the temperature of 293 K. With a molecular weight of 563 g mol^{-1}, the relaxation time yields approximately 11.19 ns, which has good agreement with the result of the MD simulation. It should be noticed that the relaxation time is essential in MD simulations due to calculating the minimum required run time and likewise diagnosing Newtonian and non-Newtonian regimes.

3.2 Wall Slip

Determining the slip length for a lubrication system is challenging in MD simulation, due to the difficulties of attaining a steady state. Although the slip velocitiy values have fluctuations with run times in this simulation, the wall slip was achieved after the simulation which was longer than 20 ns. The real shear rates were in the range of the 10^7–10^8 s^{-1}, which was estimated from the Couette velocity profile slope. When the upper wall has started to move, atoms adjacent to the moving wall either stick to it or hold, bouncing when facing it, picking up momentum to keep going with the moving surface. Therefore, the liquid has a steady flow x-direction momentum; however, the x-direction momentum will decay by other atoms jumping off further away from the upper wall.

Fig. 6 shows the velocity profile for the three different molecule structures of 1-decane. It should be noted that the slip velocities for the 1-decane trimer and tetramer are much larger than that for the 1-decane dimer. Furthermore, at this temperature and gap size, the wall slips for the 1-decane trimer and tetramer molecules were roughly equal. There is considerable variance between the wall sliding of the 1-decane dimer and those of the trimer and tetramer. The difference between these three molecule structures is more related to the molecular

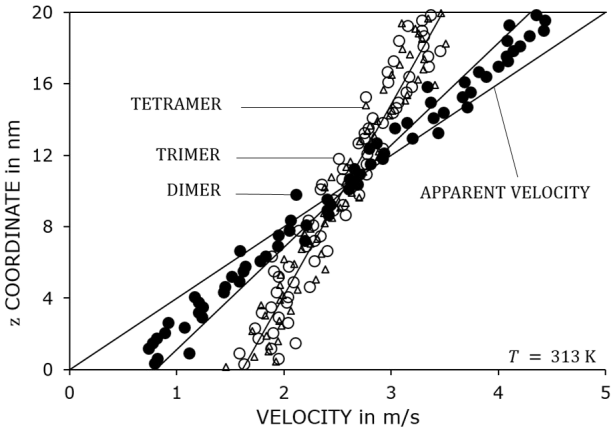

Figure 6. Couette velocity profiles of the three different branched molecule structures of 1-decane.

weight. The molecular weight of the tetramer is twice that of a dimer molecule. For the dimeric molecules, the slip velocity was about 17 % of the wall velocity at $T = 313$ K, while this value for the trimeric or tetramer molecules was about 35 %. For instance, from another MD research on hexadecane oil at a gap height of 20 nm and $T = 300$ K, the wall slip velocity was only 14 % of the wall velocity [5]. It can be stated that 1-decane molecules, which are the main components of PAO lubricants, are more efficient oils for reducing friction.

Fig. 7 shows the Couette velocity profiles across the 1-decane trimer molecules confined between iron surfaces at different temperatures. As was expected, with increasing temperature, the wall slip decreases. These results demonstrate that the wall slip depends on the temperature, indicative of the Arrhenius law. This phenomenon can be described as follows: The molecular layers of fluid flowing past each other provide insight into why the wall slip decreases with the temperature. As the PAO oil atoms of the upper layers jostle past those in the lower layers, they are all jiggling around due to thermal energy. This action helps them to split free if they are temporarily jammed upon each other. In the meantime, when the temperature increases, the molecules jiggle more violently, free themselves

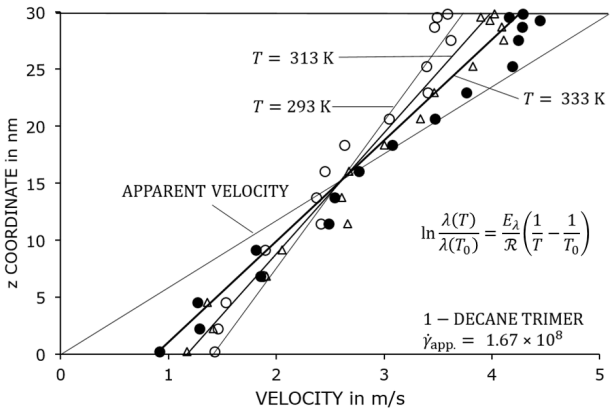

Figure 7. Velocity profiles of the 1-decane trimer at different temperatures.

more quickly, and the lubricant oil film flows faster in the upper layers, and thus the viscosity decreases.

In a macroscopic view, it is stated that the viscosity converts the flow kinetic energy into heat. Also, heat is the energy of the stochastic movement of fluid molecules. Accordingly, it is necessary to understand liquid layers sliding through each other, as observed on the molecular level, to perceive how this energy transfer occurs. Increasing the temperature means that more momentum was wasted to absorb the molecules neighboring the stationary surface. Hence, the transitional movement of the molecules in the layers near the stationary wall will drop. The lubricant, which was confined between the metal surfaces, has fewer molecular layers at a more elevated temperature. This creates the shear stress between the lubricated sliding metal surfaces. The relationship between the lubricant temperature and the wall energy is vastly complicated. It is due to the counteracting effects of the heat production by lubricant shear stress and the interfacial thermal resistance. During the surface energy increase, the lubricant is shearing with a higher shear rate due to the decline in the wall slip. Furthermore, because of the slow dynamics, the NEMD simulation of molecules at low temperatures required more calculation time.

The study on the effects of the increasing molecule branches on the wall slip showed that, with increasing molecule branching, both the slip and the shear stress increase. In this section, the effect of mixing molecules with three different numbers of branches was compared to that of a single three-branched molecule, i.e., a trimeric molecule. As can be seen in Fig. 8, the slip velocity for the mixture liquid is reduced in comparison to the liquid with only trimeric 1-decane molecules. This means that the fluid molecules near the wall have received less momentum and the wall slip has been reduced. To better understand this phenomenon, it is helpful to investigate the behavior of various PAO lubricant molecules. The various branches of the 1-decane molecules in a mixture liquid have different performances than when they are analyzed separately. The higher branched molecules showed more involvement and produced lower sliding performance. The fewer branches a molecule has, the more easily it can entangle with the carbon branches of other molecules, which causes a molecule with fewer branches in the mixture to have less movement.

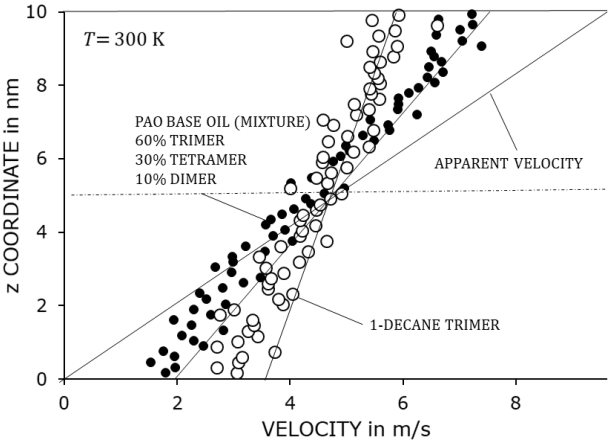

Figure 8. Velocity profile of the PAO base oil (mixture of 1-decane trimer (60 %) + tetramer (30 %) + dimer (10 %)) in comparison with the 1-decane trimer, confined between smooth iron surfaces.

While the slip length at the liquid-solid interface has been discussed in some research works, there is insufficient quantitative empirical data for submicron- or nanoscale gap heights in liquid-metal interaction. In an experimental research that studied hexadecane oil flows through nanoscale channels, the slip length values were in the range of 20–30 nm, which can be stated as a good similarity with the MD results in the present work [16]. According to our results, the slip length for the PAO-iron system yielded a maximum value of 40 nm. However, the MD results were ten times smaller than the estimated value by the experimental research of a PAO 6-steel system [17]. That experimental study applied an indirect integral technique by measuring the torque to determine the slip length of PAO 6 confined between nitrided stainless-steel surfaces with a roughness of 10 nm, whereas the calculation of the slip length in the current paper was by the Couette velocity profile. Although this realistic system involves thermal vibration of the metal surface atoms and also the existence of carbon atoms in steel material, both are reasons for higher slip length values.

4 Summary and Conclusion

This paper investigated the shear flow of PAO oils between two smooth iron surfaces. It presents the effects of three different branched molecule structures of 1-decane on the wall slip in interaction with the iron surfaces. Due to its relatively low computational cost, the UA model enabled the capture of molecular trends in tribological modeling of large and complex systems. In order to demonstrate that the results obtained in the MD simulations represent a technical lubrication system, an appropriate force field including different potential functions for van der Waals and bonded energies was selected for the branched hydrocarbon oil. The density and viscosity values of the PAO oil were verified for more reliability of the simulation results. A Couette velocity profile estimated the slip length values, and the velocity profiles were linear.

The results revealed that the wall slip highly depends on the molecular mass and structure. It is concluded that increasing the number of branches increases the wall slip and viscosity, in agreement with the previous MD simulations [1]. The viscosity calculation showed that the critical shear rate decreases with increasing branches. With increasing the number of molecule branches as well as the molecular mass, the relaxation time of the molecule is elevated. Besides, it was observed that the slip velocity increased with decreasing temperature. This effect means that 1-decane molecules can show different lubrication efficiencies based on the temperature. According to the MD results, the slip length increases when the temperature decreases, indicating an Arrhenius process. This finding was also confirmed in an empirical investigation by Pelz et al. [17]. However, it should be noticed that this is not a general conclusion for any tribology system. Some tribology systems consist of a fluid-solid interface in which the wall slip is independent of the temperature [18]. In addition, the wall slip for the mixture of three kinds of branched molecules of PAO was

reduced in comparison to the simulation of a system that included only 1-decane trimer molecules.

Acknowledgments

We kindly acknowledge the financial support by the German Research Foundation (DFG) within the Collaborative Research Centre 1194 "Interaction of Transport and Wetting Processes" – Project-ID 265191195, sub-project C06. The computing time was granted by Lichtenberg HPC computer resources at TU Darmstadt. We appreciate the Hessian Competence Center for High-Performance Computing – funded by the Hessen State Ministry of Higher Education, Research, and the Arts – for helpful advice. Open Access funding enabled and organized by Projekt DEAL.

The authors have declared no conflict of interest.

Symbols used

E_λ	[kg m^{-2}s^{-2}]	wall slip activation energy
h	[m]	gap height
k	[kg m^{-2}]	friction factor
M	[kg mol^{-1}]	molecular mass
r	[s]	relaxation time
T	[°C, K]	temperature
U	[m s^{-1}]	wall velocity

Greek symbols

$\dot{\gamma}$	[s^{-1}]	shear rate
ε	[kg m^{-2}s^{-2}]	interaction energy parameter
λ	[m]	slip length
μ	[kg m^{-1}s^{-1}]	dynamic viscosity
ρ	[kg m^{-3}]	density
σ	[m]	van der Waals radius
τ_{app}	[kg m^{-1}s^{-2}]	apparent shear stress

Abbreviations

EAM	embedded-atom method
LJ	Lennard-Jones
MD	molecular dynamics
NEMD	non-equilibrium molecular dynamics
NVE	constant-energy, constant-volume ensemble
PAO	polyalphaolefin
UA	United-Atom

References

[1] S. Mehrnia, P. F. Pelz, *J. Mol. Liquids* **2021**, *336*, 116589. DOI: https://doi.org/10.1016/j.molliq.2021.116589
[2] D. Savio, N. Fillot, P. Vergne, M. Zaccheddu, *Tribol. Lett.* **2012**, *46*, 11–22. DOI: https://doi.org/10.1007/s11249-011-9911-6
[3] M. A. Ghaffari, Y. Zhang, S. Xiao, *J. Micromech. Mol. Phys.* **2017**, *2*, 2. DOI: https://doi.org/10.1142/S2424913017500096
[4] J. P. Ewen, S. K. Kannam, B. D. Todd, D. Dini, *Langmuir* **2018**, *34*, 3864–3873. DOI: https://doi.org/10.1021/acs.langmuir.8b00189
[5] A. Jabbarzadeh, J. D. Atkinson, R. I. Tanner, *J. Chem. Phys.* **1999**, *110*, 2612–2620. DOI: https://doi.org/10.1063/1.477982
[6] M. D. Hanwell, D. E. Curtis, D. C. Lonie, T. Vandermeersch, E. Zurek, G. R. Hutchison, *J. Cheminf.* **2012**, *4*, 17. DOI: https://doi.org/10.1186/1758-2946-4-17
[7] L. Martínez, R. Andrade, E. G. Birgin, J. M. Martínez, *J. Comput. Chem.* **2009**, *30 (13)*, 2157–2164. DOI: https://doi.org/10.1002/jcc.21224
[8] S. Plimpton, *J. Comput. Phys.* **1995**, *117*, 1–19. DOI: https://doi.org/10.1006/jcph.1995.1039
[9] H. Berro, N. Fillot, P. Vergne, T. Tokumasu, T. Ohara, G. Kikugawa, *J. Chem. Phys.* **2011**, *135*, 134708. DOI: https://doi.org/10.1063/1.3644938
[10] S. K. Natha, R. Khare, *J. Chem. Phys.* **2001**, *115*, 10837–10844. DOI: https://doi.org/10.1063/1.1418731
[11] S. K. Natha, B. Banaszak, *J. Chem. Phys.* **2001**, *114*, 3612–3617. DOI: https://doi.org/10.1063/1.1343487
[12] M. S. Daw, M. I. Baskes, *Phys. Rev. B* **1984**, *29*, 64437. DOI: https://doi.org/10.1103/PhysRevB.29.6443
[13] A. P. Thompson, S. J. Plimpton, W. Mattson, *J. Chem. Phys.* **2009**, *131*, 154107. DOI: https://doi.org/10.1063/1.3245303
[14] P. Liu, J. Lu, H. Yu, N. Ren, *J. Chem. Phys.* **2017**, *147*, 084904. DOI: https://doi.org/10.1063/1.4986552
[15] P. Panwar, P. Michael, M. Devlin, A. Martini, *Lubricants* **2020**, *12*, 102. DOI: https://doi.org/10.3390/lubricants8120102
[16] J.-T. Cheng, N. Giordano, *Phys. Rev. E* **2002**, *65*, 031206. DOI: https://doi.org/10.1103/PhysRevE.65.031206
[17] P. F. Pelz, T. Corneli, S. Mehrnia, M. Kuhr, *J. Fluid Mech.* **2022**, *948*, A8. DOI: https://doi.org/10.1017/jfm.2022.629
[18] Z. Guo, T. S. Zhao, Y. Shi, *Phys. Rev. E* **2005**, *72*, 036301. DOI: https://doi.org/10.1103/PhysRevE.72.036301

